Rayleigh-Bénard Convection near the Gas-Liquid Critical Point

Michel Assenheimer and Victor Steinberg
Department of Nuclear Physics, The Weizmann Institute of Science, Rehovot 76100, Israel
(Received 12 March 1993)

We present experimental results on Rayleigh-Bénard convection in SF_6 near the gas-liquid critical point. We measured the critical temperature difference for the onset of convection, ΔT_0, as a function of the reduced average temperature $\tau = (\overline{T} - T_c)/T_c$ and found $\Delta T_0 = 525 \times \tau^{1.89}$, which is close to the expected power law behavior. The strong temperature dependence of the physical properties is used to scan the Prandtl number in a wide range. A new, many "target" pattern state, initiated by a defect instability, was observed.

PACS numbers: 47.27.−i, 44.25.+f, 47.20.−k

Rayleigh-Bénard (RB) convection is a well established model system in which to quantitatively study nonlinear properties of pattern formation and dynamics, both experimentally and theoretically [1]. The system has one control parameter, the Rayleigh number $R = \frac{\beta_p g d^3 \Delta T}{\nu\kappa}$, which completely determines the onset (β_p is the isobaric thermal expansion coefficient, g the acceleration of gravity, d the thickness of the fluid layer, ΔT the temperature difference across the fluid, ν the kinematic viscosity, and κ the thermal diffusivity). Another parameter, the Prandtl number $P = \frac{\nu}{\kappa}$, defines the physical properties of the fluid. Together with R the Prandtl number describes the secondary bifurcations and pattern selection. There are two well known drawbacks of RB convection. First, the absence of an experimental system in which P can be scanned continuously in a wide range, and second, the experimental limitations which make it difficult to work with cells having a very large aspect ratio $\Gamma = D/2d$ (D is the diameter of the cell). Only in ^{3}He-^{4}He superfluid mixtures is it possible to scan the Prandtl number, P, in a range from about 0.02 to about 1 by varying the average concentration and temperature [2].

We describe in this Letter a new system where both of these drawbacks can be overcome independently. We present results on RB convection in SF_6 near its critical point [3] ($T_c = 318.7$ K, $p_c = 37.8$ bar, $\rho_c = 0.730$ g/cm^3). Since the thermodynamic and kinetic properties of fluids have a power law behavior asymptotically close to the critical point, it is easy to obtain the following asymptotic scaling behavior of the critical temperature difference for the onset of convection as a function of the reduced average temperature [4] $\tau \equiv (\overline{T} - T_c)/T_c$: $\Delta T_0 \sim \tau^{\gamma+\nu}$. Here, $\overline{T}$ is the average temperature of the fluid, γ and ν are the critical exponents of the susceptibility and the correlation length, respectively [3] ($\gamma \simeq 1.24$, $\nu \simeq 0.63$), and ΔT_0 is the critical temperature difference for the onset of convection. We have neglected the power law behavior of the shear viscosity because its singular contribution, which diverges with a small exponent ≈ 0.05, is negligible with respect to its regular contribution even very close to T_c. Usually, we keep $\Delta T_0/T_c \ll \tau$, so that the thermodynamic scaling remains valid. An obvious lower limit for ΔT_0 when $\tau \to 0$ is the adiabatic temperature gradient, given by $g\beta_p T/C_p$, which is irrelevant in our experiment [4]. For the same reason the asymptotic behavior of the Prandtl number near T_c is given by $P \sim \tau^{-\nu}$. This means that P can be changed continuously over many orders of magnitude from about 1 to practically infinity by simply adjusting $\overline{T}$ (Fig. 1). However, the strong temperature dependence of the fluid properties leads to deviations from the Boussinesq approximation (BA) in which RB convection is usually treated [1]. The deviation from this approximation can be quantitatively estimated [5] by the parameter $Q = \sum_{i=0}^{4} \gamma_i p_i$, where the γ_i's represent the nondimensional variation of the relevant fluid properties evaluated at the top and bottom temperatures, and the p_i's are linear functions of P^{-1}. The Boussinesq approximation is valid for $Q^2 \ll R_0$ (R_0 is the critical Rayleigh number). However, as many experimental [6, 7] and numerical [8] results show, at $Q \sim 1$ the deviation from the BA is already significant. This is manifested by the appearance of a backward bifurcation and hexagonal pattern

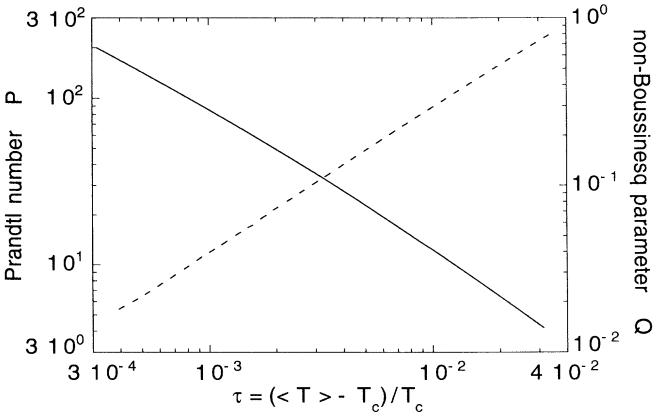

FIG. 1. Calculated values of the Prandtl number P (solid) and the non-Boussinesq parameter Q at onset (dashed) as a function of τ for $\rho = \rho_c$. The uncertainty in P is about ±10%.

near the onset as was recently clearly demonstrated [6, 7]. For a fixed value of d one obtains to leading order an asymptotic scaling for $Q \sim \tau^{\gamma+\nu-1}$. This implies that by varying $\overline{T}$, one can scan Q as well (Fig. 1). Thus, contrary to simple intuition, it is possible to work within the framework of the BA even if the fluid is near T_c.

The above presented considerations clearly illustrate the definite advantages of this system. These are the following: (a) Convection in very thin layers can be achieved close enough to T_c. Consequently, very large aspect ratio cells can be realized, which was presently only possible in electrohydrodynamic convection in nematic liquid crystals [9]. (b) P can be scanned continuously from about 1 to very large values in the same convection cell, which is crucial for the understanding of pattern selection [1]. (c) Q can also be tuned in the same manner. (d) Since convection in extremely thin cells becomes an attainable goal, two basic problems can be addressed experimentally: (1) One is the role of thermal fluctuations on pattern formation in the vicinity of the convection onset, which is decisive for our understanding of the interaction between microscopic and macroscopic degrees of freedom [10]. (2) In an extremely thin cell and close enough to the critical point, one can reach the limit of strongly fluctuating hydrodynamics, where the macroscopic length scale d is of the same order of magnitude as the thermodynamic correlation length $\xi \sim \tau^{-\nu}$. Then, the hydrodynamical description itself becomes questionable.

SF_6 was enclosed in a stainless steel vessel having a sapphire window 19 mm thick and 102 mm in diameter. A nickel plated copper bottom plate, to which a thermofoil heater was attached, sandwiched the Mylar spacer defining the side walls. The vessel was coupled by a thin tube to a small hot volume, in which pressure feedback was performed by heating the fluid. Both vessels were enclosed in a thermostated bath in which the long-term stability was better than ± 1.0 mK. Long-term stability of the bottom temperature was about ± 0.3 mK. Pressure feedback allowed for long-term stability of ± 0.5 mbar. A specially designed high spatial resolution shadowgraph and computer enhancement were used for pattern visualization. The thin cell allowed for precise direct optical detection of the convection onset. The cell was filled far from the critical point where the equation of state is more accurate [11]. The uncertainty in the desired density was about $\pm 0.25\%$. Nonuniformity of the cell was caused mainly by bending of the sapphire window, but did not exceed 1.8 μm over the diameter of the cell. The cell itself had a diameter of 30 mm, while the fluid layer thickness was estimated to be 130 μm, resulting in $\Gamma = 115$.

In Fig. 2 we present the experimental results of the critical temperature difference for the onset of convection as a function of τ for several densities. From Fig. 2 it is obvious that for reduced densities $\rho_r = \rho/\rho_c$ close to and slightly above 1, the data can be described by a simple power law, whose exponent is surprisingly close to

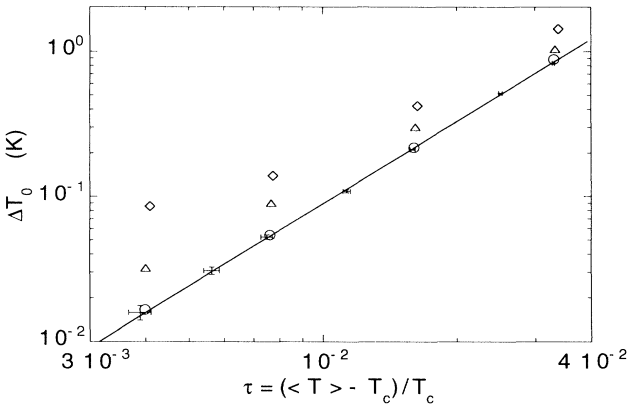

FIG. 2. Measured values of ΔT_0 as a function of τ for several reduced densities $\rho_r = 0.93$ ($\diamond$), 1.00 (dots with error bars), 1.04 ($\bigcirc$), and 1.17 ($\triangle$).

the predicted one, $\gamma + \nu$. The best fit for $\rho_r = 1.00$ gives $\Delta T_0 = (524.90 \pm 1.08) \times \tau^{1.886 \pm 0.042}$. The coefficient of the fit, which is proportional to R_0, deviates from the theoretically predicted prefactor by less than a factor of 2. The coincidence of the theoretically predicted and experimentally observed value of the exponent can be explained by a fortunate interplay between the temperature dependence of the regular nondivergent parts and the singular divergent parts of the physical parameters which contribute to ΔT_0 in the range of $3.9 \times 10^{-3} < \tau < 3.3 \times 10^{-2}$. In this range in particular, the thermal conductivity, λ, has a regular contribution of the same order of magnitude as its singular part which diverges as $C_p/\xi\eta$ (η is the shear viscosity). The discrepancy of the prefactor, on the other hand, is also due to the uncertainties of the physical parameters forming R. Critical behavior on thermodynamic paths where $\rho \neq \rho_c$ may be accounted for by the inclusion of an additional field and leads to corrections to scaling and rounding of the divergences [3]. This is obvious from the data for $\rho_r \neq 1$ and especially striking for $\rho_r = 1.17$, since in general $\Delta T_0 \sim \rho^{-2}$. The behavior of ΔT_0 indicates that thermodynamical critical scaling can be applied to systems far from equilibrium (provided $\Delta T_0/T_c \ll \tau$), and that convection in much thinner cells close enough to T_c becomes attainable. The results on convection in a cell of about 20 μm will be published elsewhere.

As pointed out, by modifying τ we change both P and Q, which allows us to study pattern selection and non-Boussinesq behavior in a single cell. In Fig. 3 we present a plot of R/R_0 vs P. We studied the pattern selection at the critical density for four values of τ in a limited range of R. The experimental path is from ΔT_0 to $\Delta T_{\max}$ at τ approximately constant, leading to small variations in P. Since Q is roughly proportional (through the power law dependence of the physical properties) to ΔT, a significant variation in Q exists. Also shown in Fig. 3 are

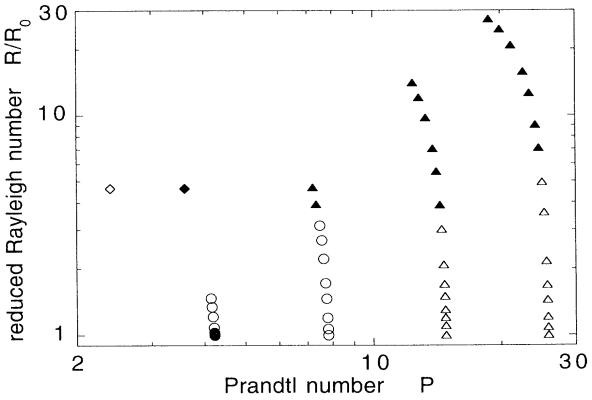

FIG. 3. Observed patterns at $\rho_r = 1.00$ as a function of R/R_0 and P: hexagons (•); rolls without defects (○); roll patches and/or rolls having defects (△); target patterns (▲). The values of τ at onset with increasing P are $3.28 \times 10^{-2}, 1.60 \times 10^{-2}, 7.62 \times 10^{-3}$, and 3.98×10^{-3}, respectively. Target (♦) and spiral patterns (◇) obtained at $\rho_r = 1.17$ are also shown for which $\tau = 1.76 \times 10^{-2}$ and 3.92×10^{-2}, respectively.

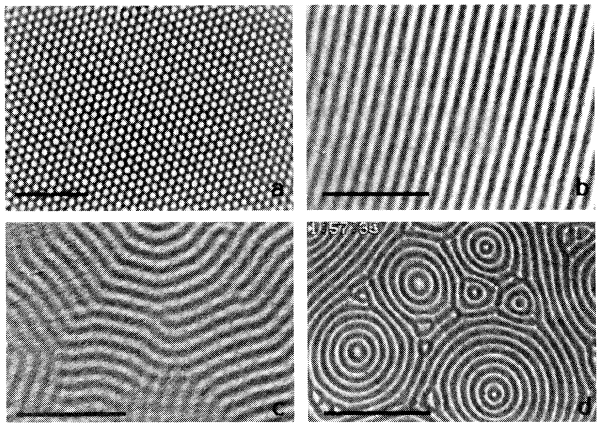

FIG. 4. Observed patterns for $\rho_r = 1.00$. The values for R/R_0, P, Q, and τ are given in brackets respectively: (a) hexagons $(1.02, 4.2, 0.78, 3.28 \times 10^{-2})$; (b) rolls $(1.08, 4.2, 0.80, 3.29 \times 10^{-2})$; (c) roll patches $(1.04, 26, 0.13, 3.98 \times 10^{-3})$; (d) target patterns $(7.04, 14, 1.6, 8.25 \times 10^{-3})$. The bar represents 1 mm.

patterns observed at $\rho_r = 1.17$ and $R/R_0 = 4.63$ for two values of P.

At the critical density for small P or large τ, hexagons were observed near the onset [Fig. 4(a)]. By increasing ΔT a hysteretic transition to straight rolls was found, as expected [6, 7]. The existence of hexagonal patterns near the onset depends on the value of Q (Fig. 1), which is determined both by τ and d. For $P \approx 8$, a continuous transition to rolls over the entire cell is observed [Fig. 4(b)]. At larger $P \approx 15$ and 25, the first patterns above the onset are disordered rolls with defects and grain boundaries [Fig. 4(c)]. The characteristic size of these roll patches becomes smaller with increasing P. At large and well-defined values of R for $P \approx 8$, 15, and 25 a transition to a new type of pattern appears [Fig. 4(d)]. These "target" patterns are initiated by a defect instability, either at a grain boundary, or in the core of a dislocation, but most often in the core of a disclination. The onset for these patterns appears for $Q \sim 1$.

Figures 5(a) and 5(b) show an instability in the core of a dislocation which is reminiscent of the bridges described by Newell and Passot [12]. Figure 5(b) illustrates how this instability initiates the breakup of a short roll. Consequently, the individual parts reconnect to eventually create a roll closed on itself [Figs. 5(c) and 5(d)]. In most cases, the core enclosed by a short circular roll becomes unstable, giving rise to an additional concentric roll [Figs. 5(e) and 5(f)]. The core, therefore, acts as a source for the circular wave, creating the target pattern. At $\Delta T_{\max}$ spatiotemporal chaotic behavior of many target patterns in the cell was observed. We observed target patterns for a wide range of P numbers for large enough ΔT, where Q becomes large. We also observed a transition from a many target to a many spiral state as well as a transition from target to spiral *turbulence* [13] in the range of $P \approx 2.4$ to 3.6 for $\rho/\rho_c = 1.17$ by varying τ (or P). Both spiral and target patterns appear at large enough Q, which indicates that these patterns are intrinsic to non-Boussinesq systems, while the region

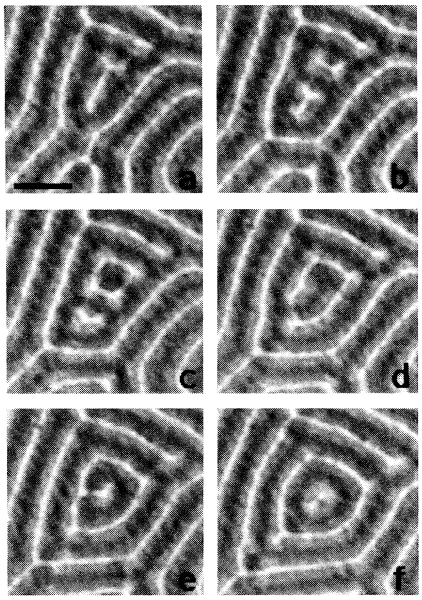

FIG. 5. One of the scenarios of target formation. The parameters are $P = 14.1$, $R/R_0 = 5.53$, $Q = 1.43$, and $\tau = 8.08 \times 10^{-3}$. Time between frames: $12\tau_v$ ($\tau_v = d^2/\kappa = 4.7$ s is the vertical diffusion time). The bar represents 200 μm.

of stability of the patterns depends on the value of P. Recently, it was shown both experimentally [7] and numerically [8] that non-Boussinesq effects are essential to spiral patterns. As is obvious from Fig. 3, target patterns are stable for large values of P, while the spiral patterns are stable in the low P regime.

Since curved rolls appear at large P and large Q, one can conclude that nonvariational effects become significant in this range of parameters. There are two sources for nonvariational effects: one due to large scale flow which is inversely proportional [14] to P and one due to strong deviations from the BA [15]. The appearance of curved rolls at large P definitely indicates that the second type of nonvariational effect is crucial here.

In conclusion, we have illustrated that RB convection near the critical point is an advantageous system in which to study pattern selection in a wide range of P and Q. New target shaped patterns and target turbulence have been observed. These patterns are initiated by a novel defect core instability mechanism. A quantitative study of this instability will be presented elsewhere.

This work was partially supported by the U.S.–Israeli Binational Scientific Foundation (BSF) Grant No. 90-00412, the Israel Science Foundation, and the German Israel Foundation Grant No. I-130091.

[1] P. Manneville, *Dissipative Structures and Weak Turbulence* (Academic, New York, 1990).
[2] V. Steinberg, Phys. Rev. A **24**, 975 (1981).
[3] J. V. Sengers and J. M. H. Levelt Sengers, in *Progress in Liquid Physics*, edited by C. A. Croxton (Wiley, New York, 1978), references therein.
[4] M. Gitterman and V. Steinberg, High Temperature (USSR) **8**, 754 (1970); for a review, see M. Gitterman, Rev. Mod. Phys. **50**, 85 (1978).
[5] F. H. Busse, J. Fluid Mech. **30**, 625 (1967).
[6] S. Ciliberto, E. Pamploni, and C. Pérez-Garcia, Phys. Rev. Lett. **61**, 1198 (1988).
[7] E. Bodenschatz, J. R. de Bruyn, G. Ahlers, and D. S. Cannell, Phys. Rev. Lett. **67**, 3078 (1991).
[8] H. Xi, J. Viñals, and J. D. Gunton, Phys. Rev. A **46**, R4483 (1992).
[9] I. Rehberg, S. Rasenat, and V. Steinberg, Phys. Rev. Lett. **62**, 756 (1989). Recently, an aspect ratio of $\Gamma = 86$ was reached in RB convection in a compressed gas (see [7]).
[10] M. C. Cross and P. C. Hohenberg, Rev. Mod. Phys. (to be published).
[11] T. E. Morsy, J. Chem. Eng. Data **15**, 256 (1970).
[12] A. C. Newell and T. Passot, Phys. Rev. Lett. **68**, 1846 (1992).
[13] S. W. Morris, E. Bodenschatz, D. S. Cannell, and G. Ahlers, Bull. Am. Phys. Soc. **37**, 1734 (1992).
[14] E. D. Siggia and A. Zippelius, Phys. Rev. Lett. **47**, 835 (1981).
[15] H. R. Brand, Prog. Theor. Phys. Suppl. **99**, 442 (1989).

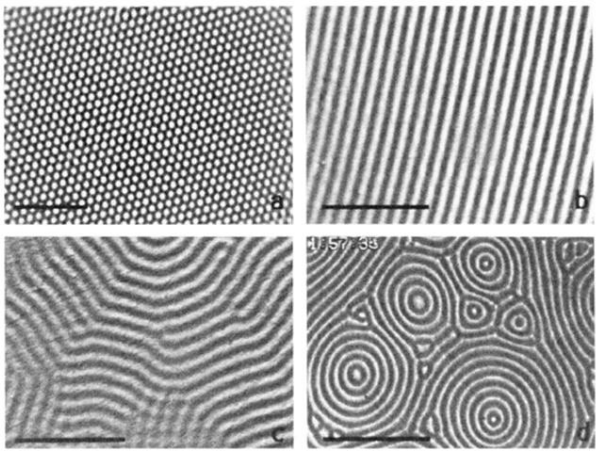

FIG. 4. Observed patterns for $\rho_r = 1.00$. The values for R/R_0, P, Q, and τ are given in brackets respectively: (a) hexagons $(1.02, 4.2, 0.78, 3.28 \times 10^{-2})$; (b) rolls $(1.08, 4.2, 0.80, 3.29 \times 10^{-2})$; (c) roll patches $(1.04, 26, 0.13, 3.98 \times 10^{-3})$; (d) target patterns $(7.04, 14, 1.6, 8.25 \times 10^{-3})$. The bar represents 1 mm.

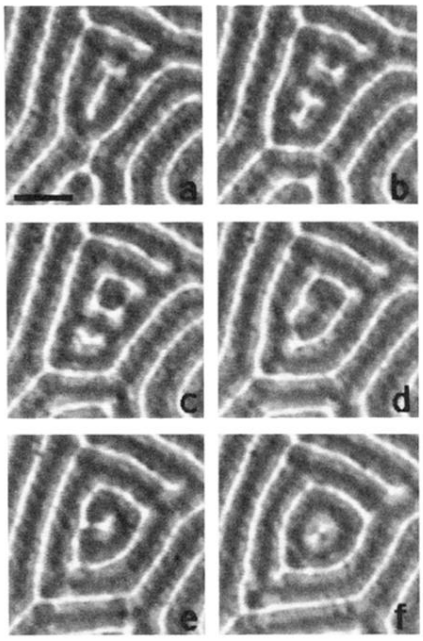

FIG. 5. One of the scenarios of target formation. The parameters are $P = 14.1$, $R/R_0 = 5.53$, $Q = 1.43$, and $\tau = 8.08 \times 10^{-3}$. Time between frames: $12\tau_v$ ($\tau_v = d^2/\kappa = 4.7$ s is the vertical diffusion time). The bar represents 200 μm.